Cell Reports

Article

A platform of functional studies of ESCC-associated gene mutations identifies the roles of TGFBR2 in ESCC progression and metastasis

Graphical abstract

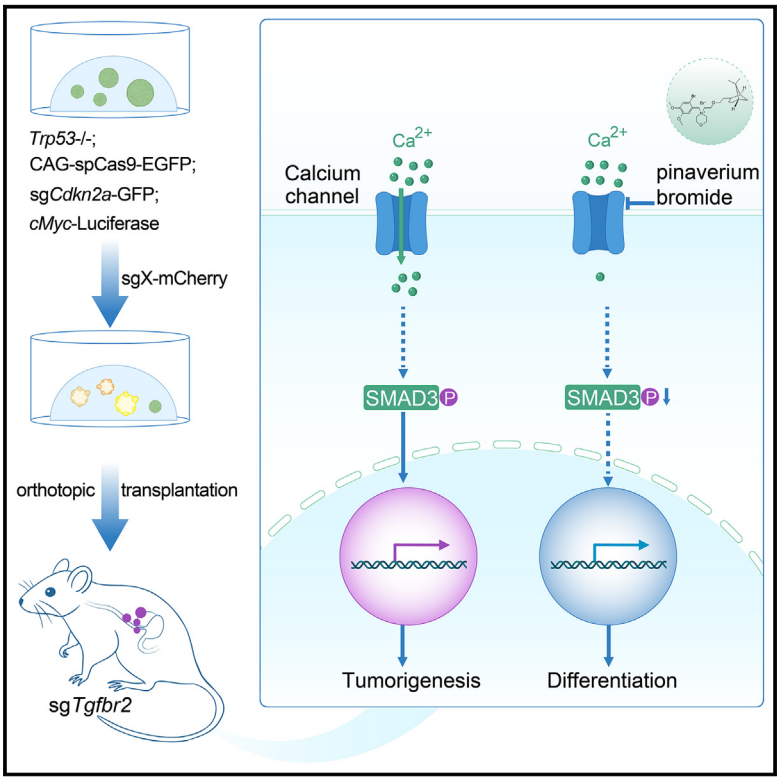

Highlights

- Primary ESCC mouse models were generated with genetically engineered esophageal organoids
- CRISPR-Cas9 screening confirmed the functions of multiple tumor-suppressor genes in ESCC
- *Tgfbr2* loss promotes ESCC progression and metastasis through *Smad3*
- Pinaverium bromide reduces the growth of *Tgfbr2*-deficient ESCC by reducing SMAD3

Authors

Jian Wang, Jiajia Du, Xiangmeng Luo, ..., Yu Liu, Feifei Na, Chong Chen

Correspondence

drchenlq@scu.edu.cn (L.C.), hubingnj@163.com (B.H.), yuliuscu@scu.edu.cn (Y.L.), nafeifei@scu.edu.cn (F.N.), chongchen@scu.edu.cn (C.C.)

In brief

Wang et al. generate a series of primary ESCC mouse models driven by different genetic mutations with premalignant esophageal organoids. Among them, TGFBR2-deficient ESCC, in which *Smad3* activation is abnormally activated, can be targeted by pinaverium bromide, an FDA-approved calcium channel blocker.

Wang et al., 2024, Cell Reports *43*, 114952
November 26, 2024
https://doi.org/10.1016/j.celrep.2024.114952

CellPress

Cell Reports

CellPress
OPEN ACCESS

Article

A platform of functional studies of ESCC-associated gene mutations identifies the roles of TGFBR2 in ESCC progression and metastasis

Jian Wang,[1,8] Jiajia Du,[1,8] Xiangmeng Luo,[1,8] Linjie Guo,[1,8] Yixin Liu,[2,8] Jianfeng Zhou,[2] Yang Zou,[1] Zhenghao Lu,[3] Xiangyu Pan,[1] Xuelan Chen,[1] Ailing Zhong,[1] Xudong Wan,[1] Lu Wang,[1] Hongyu Liu,[1] Siqi Dai,[1] Shiyu Zhang,[4] Xingyu Xiong,[4] Ping Tan,[4] Manli Wang,[1] Baohong Wu,[1] Qi Zhang,[1] Yingjie Wang,[1] Mengsha Zhang,[1] Runda Lu,[2] Huahang Lin,[2] Yuan Li,[1] Yaxin Li,[1] Zongkai Han,[1] Longqi Chen,[2,*] Bing Hu,[1,*] Yu Liu,[1,*] Feifei Na,[6,*] and Chong Chen[1,5,7,9,*]
[1]Department of Gastroenterology, State Key Laboratory of Biotherapy and National Clinical Research Center for Geriatrics, West China Hospital, Sichuan University, Chengdu, Sichuan 610041, China
[2]Department of Thoracic Surgery, West China Hospital, Sichuan University, Chengdu, Sichuan 610041, China
[3]Chengdu OrganoidMed Medical Laboratory, West China Health Valley, Chengdu, Sichuan 610041, China
[4]Department of Urology, Institute of Urology, West China Hospital, Sichuan University, Chengdu, Sichuan 610041, China
[5]Frontiers Medical Center, Tianfu Jincheng Laboratory, No387-201 Hemin st., Chengdu, Sichuan 610212, China
[6]Department of Thoracic Oncology, West China Hospital, Sichuan University, Chengdu, Sichuan 610041, China
[7]Children's Medicine Key Laboratory of Sichuan Province, Sichuan 610041, China
[8]These authors contributed equally
[9]Lead contact
*Correspondence: drchenlq@scu.edu.cn (L.C.), hubingnj@163.com (B.H.), yuliuscu@scu.edu.cn (Y.L.), nafeifei@scu.edu.cn (F.N.), chongchen@scu.edu.cn (C.C.)
https://doi.org/10.1016/j.celrep.2024.114952

SUMMARY

Genomics studies have detected numerous genetic alterations in esophageal squamous cell carcinoma (ESCC). However, the functions of these mutations largely remain elusive, partially due to a lack of feasible animal models. Here, we report a convenient platform with CRISPR-Cas9-mediated introduction of genetic alterations and orthotopic transplantation to generate a series of primary ESCC models in mice. With this platform, we validate multiple frequently mutated genes, including *EP300*, *FAT1/2/4*, *KMT2D*, *NOTCH2*, and *TGFBR2*, as tumor-suppressor genes in ESCC. Among them, *TGFBR2* loss dramatically promotes tumorigenesis and multi-organ metastasis. Paradoxically, *TGFBR2* deficiency leads to *Smad3* activation, and disruption of *Smad3* partially restrains the progression of *Tgfbr2*-mutated tumors. Drug screening with tumor organoids identifies that pinaverium bromide represses Smad3 activity and restrains *Tgfbr2*-deficient ESCC. Our studies provide a highly efficient platform to investigate the *in vivo* functions of ESCC-associated mutations and develop potential treatments for this miserable malignancy.

INTRODUCTION

Esophageal squamous cell carcinoma (ESCC) is one of the most lethal malignancies, especially in East Asia, including China, where about 90% of ESCC cases occur.[1,2] The outcomes of patients with ESCC have remained poor during the past decades, and our understanding of its underlying molecular mechanisms is limited.

In recent years, several genomics studies found numerous genetic alterations, including gene mutations and chromosome copy-number and structural variations.[3–5] Among them, *TP53* is the most frequently mutated gene, which is disrupted in about 90% ESCC cases. Other highly mutated genes include *CDKN2A*, *PTEN*, *RB1*, *NOTCH1*, *KMT2D*, and *FAT1/2/3/4*, while oncogenic *MYC*, *CCND1*, and *PIK3CA* are amplified or overexpressed.[3,6–8] However, intriguingly, there is accumulating evidence indicating that histologically normal esophageal epithelial cells also contain a lot of mutations and that many of them overlap with those in ESCC.[9,10] These findings raise the urgent need to dissect the biological functions of these ESCC-associated genetic alterations in the initiation, progression, and clinic treatment of this disease. It has been reported that *p53* mutations and the following loss of heterozygosity promote clonal expansion and chromosomal instability of esophageal epithelial cells.[11] Instead, *NOTCH1* mutations give rise to a clonal competitive advantage of normal esophageal epithelial cells over wild-type ones but restrain tumor progression.[12] Most of the other ESCC-related mutations need further investigations.

Animal models, such as genetically engineered mouse models (GEMMs), which are driven by defined genetic mutations and able to recapitulate the process of ESCC genesis from the normal esophageal epithelial cells to fully transformed tumors, are necessary for studying the molecular mechanisms underlying ESCC.[13] However, unfortunately, ESCC GEMMs are less

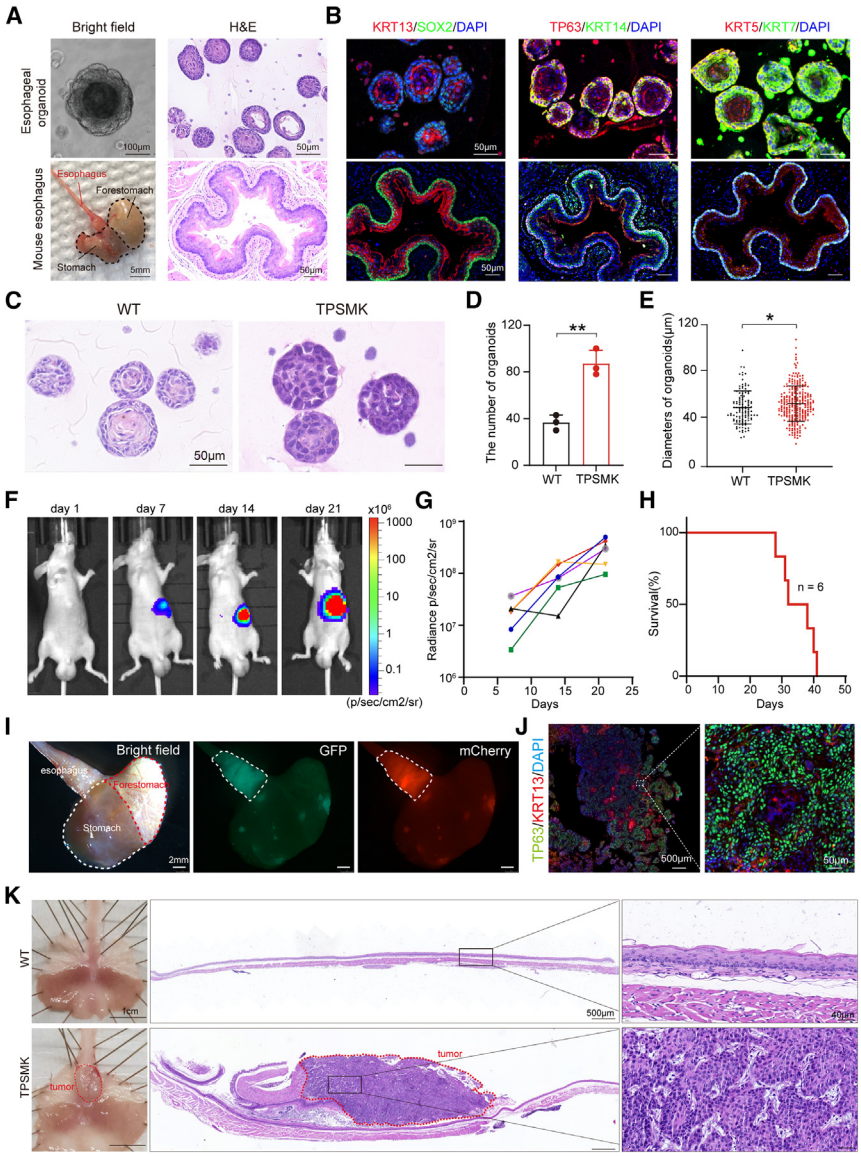

Figure 1. Generating an OPCM for ESCC by orthotopically transplanting gene-edited esophageal organoids in mice

(A) Representative bright-field (left) and hematoxylin and eosin (H&E) staining (right) images of the murine esophagus (bottom) and parallel organoids (top). Scale bars, 100 μm (bright field, top), 5 mm (bright field, bottom), and 50 μm (H&E).

(B) Representative immunofluorescence co-staining images of SOX2 and KRT13, TP63 and KRT5, and KRT5 and KRT7 in the esophagus (bottom) and organoids (top). Scale bars, 50 μm.

(C) Representative H&E staining pictures of wild-type (WT) (left) and gene-edited (right) organoids with the combination of *Trp53*$^{-/-}$; sg*Pten*; sg*Smad4*; *Myc*; *Kras*^{G12D} (TPSMK). sgRNA, single-guide RNA; scale bars, 50 μm.

(D) Bar plots show the number of organoids per view in WT and TPSMK organoids. Data are the mean of three biological repeats, and error bars show ±SD. $^{**}p < 0.001$, unpaired t test.

(E) Scatterplot quantification of the diameters of WT and TPSMK organoids. Data are the mean of three biological repeats, and error bars show ±SD. $^{*}p < 0.05$, unpaired t test.

(F and G) Representative living images showing the orthotopic tumor growth in TPSMK OPCMs (F). Line chart showing the D-luciferase fluorescence intensity at 7, 14, and 21 days after transplantation, $n = 6$ (G).

(H) The survival curve of recipient mice with TPSMK organoids, $n = 6$.

(I) Representative images of bright field (left), green fluorescence (middle), and red fluorescence (right) in esophagus of TPSMK OPCM mice. Scale bar, 2 mm.

(J) Representative immunofluorescence co-staining images of TP63 and KRT13 in TPSMK tumor tissue. Scale bars, 500 μm (left) and 50 μm (right).

(K) Representative TPSMK gastroesophageal tumor and WT tissue pictures (left) and overview of longitudinal section of H&E staining. Scale bars, 1 cm (left), 500 μm (middle), and 40 μm (right).

developed, partially due to the esophageal-epithelium-specific Cre missing.[14] Recently, our group and others developed an alternative strategy by *in situ* transplanting gene-edited normal epithelial organoids to generate primary, orthotopic, and genetics-defined tumor models, named the OPCM (organoid-initiated precision cancer model). Compared to GEMMs, the OPCM can be applied for all types of cancers and is convenient to study any gene mutation or combination of multiple mutations. OPCMs have been generated for various cancers, such as lung cancer,[15] gastric cancer,[16] colorectal cancer,[17] and endometrial cancer,[18] with different genetic drivers. Here, we further develop primary and orthotopic OPCMs of ESCC and systematically investigate the *in vivo* functions of the top 20 most frequently mutated genes in ESCC. The results validated multiple ESCC driving mutations, including the loss of *Kmt2d*, *Fat1/2/4*, *Notch2*, and *Tgfbr2*. Among them, ESCC with *Tgfbr2* deficiency displayed massive distal metastasis, and its susceptibility was explored. Our study provides a platform to dissect the molecular mechanisms underlying ESCC pathogenesis.

RESULTS

Generating an OPCM for ESCC with gene-edited organoids of normal esophagus in mice

We sought to generate primary, orthotopic, and driver-defined ESCC mouse models with genome-edited esophageal organoids in mice (Figure S1A). Mouse esophageal tissue was digested into single cells by trypsin, followed by a three-dimensional (3D) culture to form organoids. These aggregates demonstrated predominantly solid architecture, with observable central keratinized features, resembling the epithelial

structure of normal esophageal tissue (Figure 1A). Cellular identification was performed using epithelial cell markers KRT5 and KRT7, squamous stem cell markers SOX2 and TP63, stratified squamous epithelium basal cell marker KRT14, and differentiation marker KRT13, displaying nearly identical distribution and arrangement to native tissue (Figure 1B). After successfully establishing prolonged *in vitro* cultivation of murine esophageal organoids, genetic manipulation was carried out. In the cohort of patients with ESCC, deletions or mutations in known tumor-suppressor genes *TP53*, *PTEN*, and *SMAD4* and amplification of *MYC* and *KRAS* are common events (Figure S1B). The hypothesis was that combinations of these genotypes contribute to ESCC development. Esophageal tissues from *Trp53*$^{-/-}$; *Rosa26CAG-spCas9-IRES-eGFP* donor gene mice were isolated, and the P53 expression level was validated using western immunoblotting (Figure S1C). Genetic modifications were introduced using lentiviral vectors targeting tumor-suppressor genes and retroviral vectors overexpressing proto-oncogenes, carrying red fluorescent protein and luciferase reporter genes, respectively (Figure S1D). The overexpression efficiency of *Myc* and *Kras*^{G12D} was validated by qPCR (Figure S1E), while mutations of *Pten* and *Smad4* were confirmed via the T7E1 enzyme cleavage assay (Figure S1F). TPSMK (*Trp53*$^{-/-}$; sg*Pten*; sg*Smad4*; *Myc*; *Kras*^{G12D}) organoids lacked clear hierarchical differentiation compared to normal organoids (Figure 1C), and they demonstrated significant advantages in terms of quantity and size (Figures 1D and 1E). Successfully edited TPSMK organoids were orthotopically transplanted into nude mouse esophagus, and a live imaging assay enabled periodic monitoring of cellular growth. The results showed sustained and stable growth *in vivo* (Figure 1F), with the signal intensity quantified (Figure 1G). The survival of recipient mice was approximately 1 month due to reduced food intake (Figure 1H), and tumor cells notably occupied the regions of the esophagus (Figures 1I and 1K). Immunofluorescence (IF) staining for squamous epithelial markers in tumor tissues revealed positive staining for TP63, KRT13, KRT14, and KRT5, with the proliferation marker Ki67 also showing extensive positivity (Figures 1J and S1G). These findings demonstrate that the combination of organoid cultivation and genetic editing techniques enables the construction of a primary orthotopic ESCC mouse model, establishing a foundational platform for investigating the roles of individual genes in tumor initiation and development.

Investigating the biological functions of ESCC-associated mutations in esophageal organoids and OPCMs

Subsequently, we conducted *in vivo* screening of driver genes following the same experimental protocol. Genetic sequencing data revealed that over 20% of individuals with ESCC had concurrent mutations or deletions in *TP53* and *CDKN2A*, along with *MYC* amplification (Figure S2A). Therefore, we adopted this triad as the baseline and introduced mutations of candidate genes for subsequent experiments to validate their functions. The mutations of *Cdkn2a* (Figure S2B) and the overexpression efficiency of *Myc* were confirmed (Figure S2C).

We selected the top 20 genes with the highest frequency of aberrations (mutations, deletions, and amplifications). The histone regulator genes *KMT2D* (15%), *KMT2C* (18%), *EP300* (17%), *KDM6A* (18%), and *CREBBP* (16%) exhibited frameshift or truncation mutations at a high frequency in ESCC. Pathway assessment reveals predominant involvement in the cell cycle (*RB1* [18%], *PTCH1* [15%], and *NFE2L2* [9%]), NOTCH (*NOTCH1* [16%], *NOTCH2* [9%], *NOTCH3* [16%], and *FBXW7* [22%]), HIPPO (*FAT1* [24%], *FAT2* [34%], and *FAT4* [42%]), and PI3K (*PIK3CA* [24%] and *PTEN* [16%]) pathways. Transforming growth factor β receptor 2 (*TGFBR2*) exhibited a frequency of loss of heterozygosity combined with mutations exceeding 40% (Figure 2A). And these genes' alterations co-occurred with TP53, CDKN2A, and MYC, respectively (Figure 2B; Tables S3 and S4). *In vitro* results showed variations in organoid formation capabilities among different groups, with TGFBR2-deficient organoids achieving the highest quantity (Figures 2C and 2D). Most organoids exhibited disadvantageous size attributes (Figure 2E). Tumorigenesis is a dynamic *in vivo* process influenced by microenvironments and cytokines. There was no obvious luciferase signal 20 days after transplantation, but it did appear at 60 and 75 days in each group except the control group (Figures 2F and S2E). Unlike other gastrointestinal tumors, ESCC originates from the basal layer of squamous cells and tends to metastasize to lymph nodes in the early stages.[19] Thus, clinical symptoms could only be stimulated by an orthotopic mouse model. *In vivo* results showed that *Trp53*$^{-/-}$ sg*Cdkn2a Myc* (TCM) organoids did not give rise to malignant tumors and remained asymptomatic over 12 months. Conversely, TCM organoids with ablations of *Ep300*, *Fat1/2/4*, *Kmt2d*, and *Notch2* drive the formation of ESCC, and overall survival varies from 3 to 10 months (Figures 2G and 2H). Additionally, loss of *Ep300*, *Fat2*, and *Fat4* led to liver metastasis (Figures 2H and S2F–S2I).

Distinct pathogenesis of ESCC with different genetic drivers

Genomic analysis of samples from patients with ESCC illustrated a complex heterogeneous landscape, reflecting diverse pathological characteristics. Histopathologically, ESCC is classified into four grades: well differentiated, moderately differentiated, poorly differentiated, and undifferentiated.[20] SOX2 is critical for self-renewing stem cells and morphogenesis in the esophagus.[21] KRT14, another stem cell marker, is frequently co-expressed with SOX2 in basal membrane cells. KRT5 is expressed in the maturated squamous epithelium of the superficial layer. KRT13 is expressed in the stratified squamous epithelium and well-differentiated nests.

Despite the pathological manifestation of squamous carcinoma features observed with the loss of the mentioned driver genes, further exploration of distinctions among these tumor cells led us to subject them to conventional marker staining analyses. The results revealed the expression of squamous epithelial markers KRT14 and KRT5 and the stemness marker SOX2 across all groups. Particularly, the differentiated squamous epithelial cell marker KRT13 showed higher expression in the sg*Ep300*, sg*Fat4*, sg*Kmt2d*, and sg*Notch2* groups. Additionally, Ki67 showed higher expression in the sg*Fat4* and sg*Kmt2d* groups, while it exhibited lower expression in the

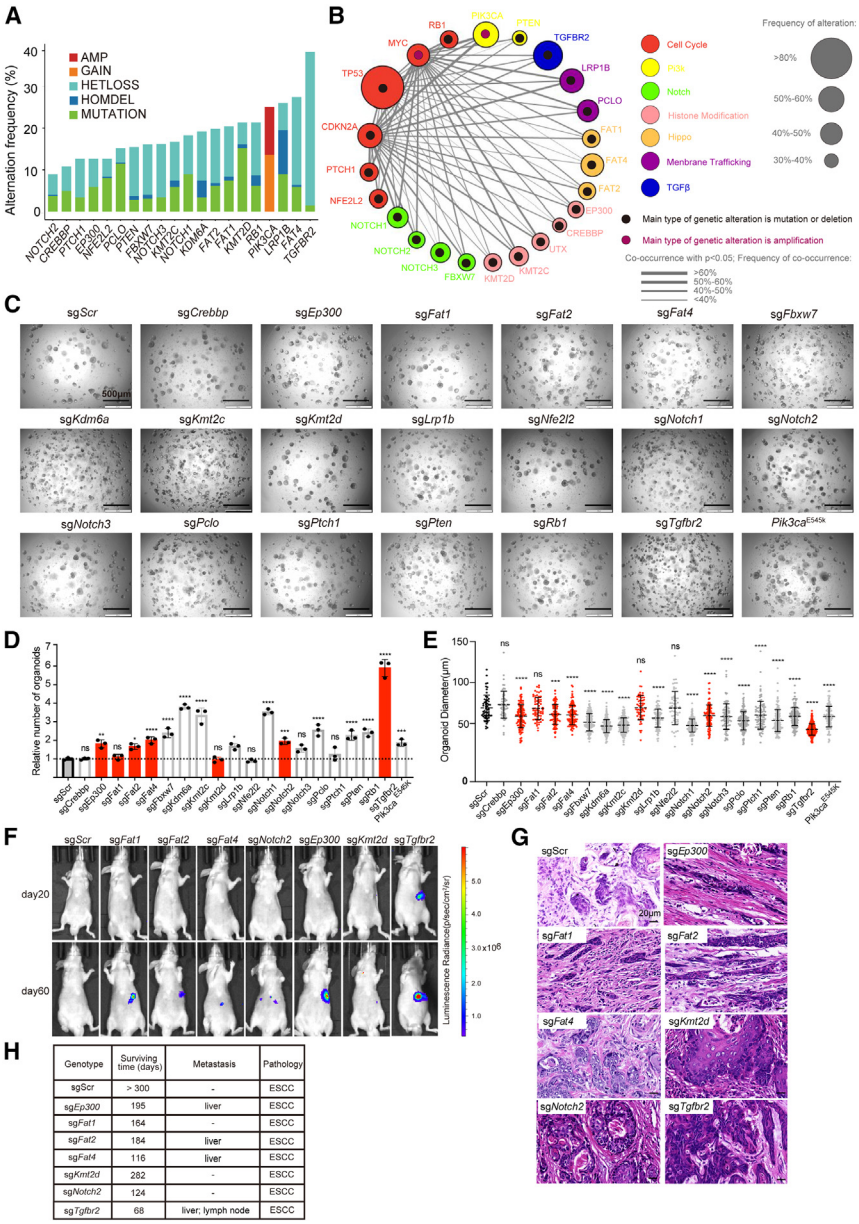

Genotype	Surviving time (days)	Metastasis	Pathology
sgScr	> 300	-	ESCC
sgEp300	195	liver	ESCC
sgFat1	164	-	ESCC
sgFat2	184	liver	ESCC
sgFat4	116	liver	ESCC
sgKmt2d	282	-	ESCC
sgNotch2	124	-	ESCC
sgTgfbr2	68	liver; lymph node	ESCC

Figure 2. Investigating the biological functions of the most frequently mutated genes in ESCC with esophageal organoids and OPCMs

(A) The histogram shows the genomic aberrations of 20 candidate genes in 323 ESCC samples from TCGA, ICGC, and UCLA studies. The types of alterations are shown in the marked colors.

(B) The networks show the co-occurrence of candidate genes.

(C) Photomicrographs of primary TCM organoids with candidate genes edited in each group. Scale bar, 100 μm.

(D) Bar plots show the relative number of TCM organoids with different mutations. Red column denotes tumorigenicity. Data are the mean of three technique repeats, and error bars show ±SD. $^{*}p < 0.05$, $^{**}p < 0.01$, $^{***}p < 0.001$, and $^{****}p < 0.0001$, ns, no significant, unpaired t test.

(E) Scatterplot quantification of the diameters of TCM organoids with different mutations. Data are the mean of three technique repeats, and error bars show ±SD. Unpaired t test.

(F) Representative living images of each group at days 20 and 60 after transplantation.

(G) Representative H&E staining pictures of TCM sgScr, sg*Ep300*, sg*Fat1*, sg*Fat2*, sg*Fat4*, sg*Kmt2d*, sg*Notch2*, and sg*Tgfbr2* tumor tissue, respectively. Scale bar, 20 μm.

(H) The statistical table summarizes the outcomes of survival time, metastasis, and pathology of tumorigenic groups.

sg*Ep300*, sg*Fat1*, sg*Fat2*, and sg*Notch2* groups (Figures 3 and S3).

ESCC with *Tgfbr2* loss displays massive distal metastasis

Aneuploidy, involving whole-chromosome or chromosome-arm imbalances, occurs in 88% of cancers.[22] Chromosome arm 3p deletion is a specific pattern in squamous carcinoma, particularly in ESCC. Notably, in targeted ESCC OPCMs, *Tgfbr2*, located at chromosome 3p, demonstrated the most significant potential for initiating tumors, resulting in the shortest latency period and facilitating extensive metastasis. Thus, we validated its function by two independent sgRNAs, respectively. These tumor cells once again exhibited an advantage in self-renewal due to the lack of *TGFBR2* expression both *in vitro* and *in vivo* (Figures 4A, 4B, and 4D). The knockout of *Tgfbr2* was identified by western blot (Figure S4A). Combined with TCM alterations, genetic ablation of *Tgfbr2* resulted in a dramatic morphological change, with a hollow structure losing the keratin layer (Figures 4A and 4C). The recipient mice with *Tgfbr2* knockout organoids developed lethal tumors within 3 months (Figure 4E). The most crucial clinical feature of ESCC is its ability to metastasize in the early stage, which is rarely observed in traditional mouse models. However, *TGFBR2*-deficient ESCC OPCMs represent lymph node invasion and distant metastasis to the liver and spleen, as frequently observed in patients. Mice harboring *Tgfbr2* knockout organoids showed a higher frequency of lymph node invasion and liver metastasis compared to those with targeted Scr (Figure 4F). Furthermore, IF staining of tumor organoids revealed significantly more robust expression of the stemness marker KRT14 and superficial marker KRT5 in *Tgfbr2* knockout versus Scr (Figure 4G). Fluorescence imaging and immunohistochemistry (IHC) staining demonstrated that these metastases originated from transplanted organoids and exhibited characteristics of ESCC (Figures S4B and S4C). Besides, in histology, tumor cells expressed high levels of KRT14 and KRT5, partially positive for

CellPress
OPEN ACCESS

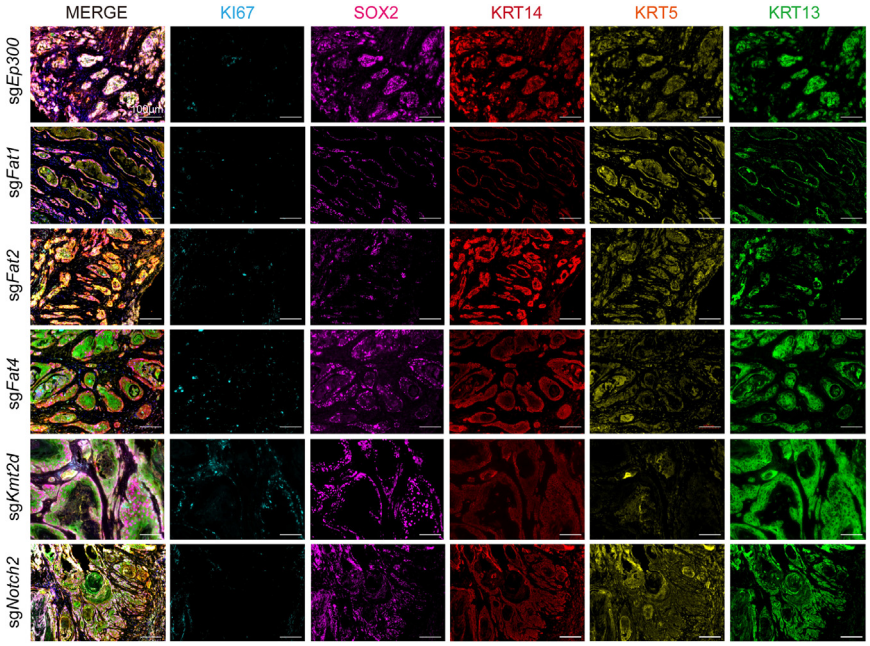

Figure 3. Distinct pathological features of ESCC with different genetic drivers

Multiplex immunohistochemical images of proliferation marker KI67 and ESCC-associated markers SOX2, KRT14, KRT5, and KRT13 in sg*Ep300*, sg*Fat1*, sg*Fat2*, sg*Fat4*, sg*Kmt2d*, and sg*Notch2* groups. Scale bar, 100 μm.

KRT13, consistent with poorly differentiated in ESCC (Figures 4H and S4B), suggesting that, in the case of *TGFBR2* loss, TCM organoids could induce poorly differentiated and metastatic ESCC.

TGFBR2 deficiency leads to an upregulation of *Smad3* expression in ESCC

The molecular features of human ESCC tumors reflect correlations with clinical outcomes.[4] In patients with ESCC, the prevalence of *TGFBR2* loss escalates in tandem with the progression of tumor stages (Figure 5A). Altered *TGFBR2* status was associated with an elevated tumor malignant signature, while its expression showed a negative correlation with the metastasis signature (Figure S5A), suggesting a potential role for *TGFBR2* loss in promoting tumor malignancy and metastasis. To investigate the relationships between *TGFBR2* loss and metastasis, we conducted bulk RNA sequencing (RNA-seq) analyses on organoids derived from OPCM tumors with or without *Tgfbr2* knockout.

Correlation enrichment analysis revealed that OPCMs driven by *Tgfbr2* knockout had similar expression patterns to human counterparts (Figure 5B). Gene set enrichment analysis (GSEA) demonstrated a significant enrichment of malignant pathways from the hallmark of cancer[23] in the condition of TGFBR2 loss, in both human and mouse models (Figure 5C). Notably, the HALLMARK_EPITHELIAL_MESENCHYMAL_TRANSITION, a well-known marker pathway associated with tumor metastasis, showed positive enrichment. RT-qPCR results showed that the epithelial marker *Cdh1* was significantly deregulated in both TCM sg*Tgfbr2* (TCMT) tumor organoids (Figure S5C). Further supporting these observations, TCMT tumors demonstrated an elevated signature associated with metastasis (Figure 5D). Intriguingly, HALLMARK_TGF_BETA_SIGNALING, a pathway with TGFBR2 as a crucial receptor implicated in tumor initiation, malignancy, and metastasis,[24] showed consistent upregulation in both mouse and human conditions of *TGFBR2* loss (Figure 5E). Multiple TGF-β signaling genes, including *Tgfb1*, *Tgfb2*, *Tgfbr1*, *Smad3*, and *Smad7*, were upregulated in TCMT, revealed by RNA-seq analyses and validated by qPCR (Figures S5B and S5F). Additionally, the protein level of phosphorylated SMAD2/3 (p-SMAD2/3) was elevated in TCMT tumor organoids (Figures 5G, S5E, and S5F). Given that *Smad3* is a transcription factor and its target genes exhibit high expression in patients with *TGFBR2* loss (Figure 5H), we performed *Smad3* knockout experiment in TCMT tumor organoids, revealing that the sg*Smad3* organoids exhibited significantly diminished growth compared to sgScr organoids. This implies that the self-renewal of *TGFBR2*-deficient tumor cells relies on the activation of SMAD3 (Figures 5I and 5J). Remarkably, the ablation of *Smad3* in TCMT OPCMs demonstrated improved overall survival (Figure 5K). Furthermore, pathological analysis of tumor tissues further indicates that *Smad3* knockout induces cellular differentiation and a decline in malignancy (Figure 5L). These data conclude that *Tgfbr2* destruction upregulated *Smad3*, which is crucial in tumor malignancy.

Identifying susceptibility of *Tgfbr2*-deficient ESCC with tumor organoids and OPCMs

Tumor organoids serve as robust platforms for drug sensitivity testing.[25] In this study, the genetically well-defined mouse tumor organoids with low mutational burden provide a unique opportunity to explore the vulnerability of *TGFBR2*-deficient tumor cells. Following KEGG analysis (Figure S6A), we selected inhibitors from specific pathways in the FDA-approved drug library, including PI3K/Akt/mTOR, MAPK, cell cycle, transmembrane transporters, TGF-β/Smad, epigenetics, and stem cells and Wnt, yielding a total of 68 drugs (Figure 6A). A primary screening identified 15 drugs with inhibition rates exceeding 50% and 7 drugs with inhibition rates exceeding 80%, including inhibitors targeting MAPK pathways (sorafenib, etc.), epigenetics (panobinostat, thioguanine), transmembrane transporters (pinaverium bromide [PB]), and stem cells and Wnt (CP21R7) (Figure 6B). Drug validation assay demonstrated that PB exhibited optimal efficacy at low concentrations and specific lethality against *TGFBR2*-deficient tumor cells *in vitro* (Figures 6B, 6C, and S6B). PB effectively suppressed tumor progression and metastasis in TCMT OPCMs (Figures 6D–6H and S6F–S6H).

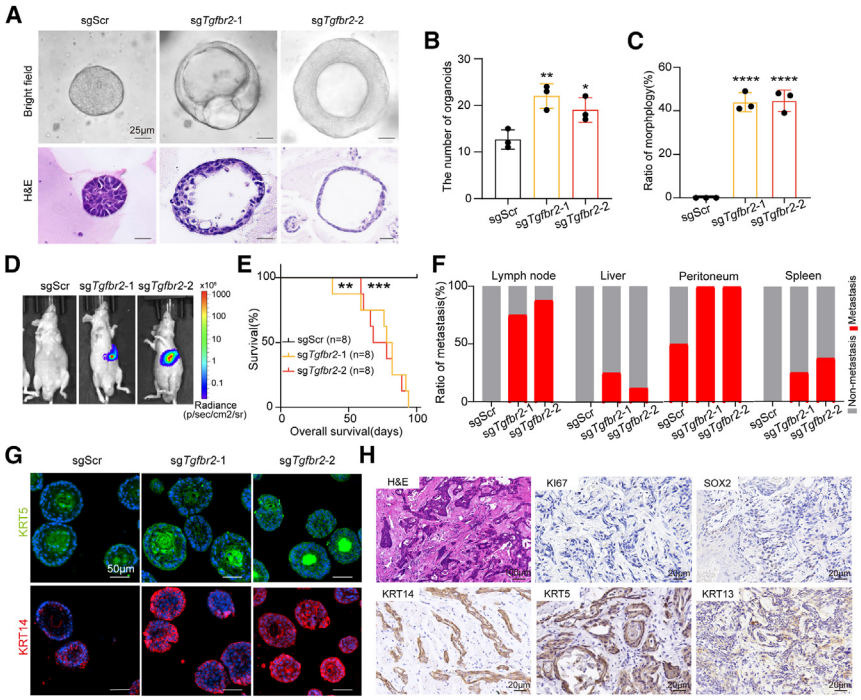

Figure 4. TGFBR2 loss promoted ESCC progression and metastasis in mice

(A) Images of bright-field (top) and H&E (bottom) staining showing the morphology of organoids after *Tgfbr2* knockout. Two independent sgRNAs were used in this experiment. Scale bar, 25 μm.

(B) Bar plot showing the number of organoid formation after *Tgfbr2* knockout. Data are the mean of three biological repeats, and error bars show ±SD. $^{*}p < 0.05$ and $^{**}p < 0.01$, unpaired t test.

(C) Bar plot showing the percentage of hollow structure organoids after *Tgfbr2* knockout. Data are the mean of three biological repeats, and error bars show ±SD. $^{****}p < 0.0001$, unpaired t test.

(D) Living images of recipient mice after engineered organoids are orthotopically transplanted.

(E) Survival of TCM OPCM mice with or without *Tgfbr2* knockout (sgScr $n = 8$; sg*Tgfbr2*-1 $n = 8$; sg*Tgfbr2*-2 $n = 8$ mice; $^{**}p < 0.01$ and $^{***}p < 0.001$ by log rank test).

(F) Bar plot showing the incidence of lymph node, liver, peritoneum, and spleen metastasis in each group (sgScr $n = 8$; sg*Tgfbr2*-1 $n = 8$; sg*Tgfbr2*-2 $n = 8$ mice).

(G) Immunofluorescence images of KRT5 (top) and KRT14 (bottom) of tumor organoids in each group. Scale bar, 50 μm.

(H) H&E staining pictures of TCMT tumor tissue and IHC pictures of KI67, SOX2, KRT14, KRT5, and KRT13. Scale bars, 100 μm (H&E) and 20 μm (IHC).

Several metastasis-related pathways were enriched in TCMT tumor organoids but downregulated by PB treatment (Figure 6I). In contrast to the vehicle group, the expression levels of TCMT-enriched signatures were also significantly reduced after PB treatment (Figure S6I). Notably, a sharp decrease in p-SMAD2/3 levels was observed within TCMT tumor organoids after PB treatment (Figure 6K). Additionally, elevated levels of the differentiation-related marker KRT13 were observed, while the expression of epithelial cell adhesion molecule (EPCAM) decreased (Figure 6J). Consistently, the scores of keratinocyte signatures were upregulated in PB-treated tumors, while the scores of unregulated p-SMADs and TCMT were downregulated (Figure 6L). Based on this, we hypothesize that calcium ion channel inhibitors contribute to inducing tumor cell differentiation by downregulating SMAD2/3 levels. More importantly, in a total of 348 patients with ESCC with hypertension, we found that patients who had been taking calcium channel blockers (CCBs) for more than 5 years had significantly better prognoses than others ($p = 0.019$) (Figure 6M). Further, we analyzed the correlation of the treatment time and the survival of the CCB-treated patients. There were a total of 219 patients with ESCC treated with CCBs, and then we stratified these patients into three groups according to the time of the treatment. The survival of the group treated for $\geq$4 years was better than that of the group treated for 2–4 years, while the survival of the group treated for 2–4 years was better than that of the group treated for $\leq$2 years, as shown in Figure 6N. These results suggest that the benefit of CCB treatment for patients with ESCC is dosage dependent and strongly support our conclusion that ESCC could be treated with CCBs.

DISCUSSION

Recently, in wild-type organoids, it was found that the introduction of specific carcinogenic mutations through genetic engineering techniques can initiate tumorigenesis, a phenomenon documented across various tissues.[15,17,26,27] However, there has been limited research on esophageal cancer using this approach. ESCC was induced through the genetic modification of normal human or murine organoids, followed by transplantation either subcutaneously or into the forestomach region of mice.[28–30] It is worth noting that these esophageal cancer models derived from organoids do not fully recapitulate the conditions of primary and orthotopic. In this study, we have established a long-term and stable culture system for mouse esophageal organoids. Following the precise editing of target genes, these organoids are directly transplanted into the mouse esophageal mucous layer, leading to the formation of esophageal tumors that closely mimic the characteristics of primary and orthotopic conditions. This innovative approach enables the rapid generation of mouse models with diverse genotypes, facilitating their application in a wide range of experimental scenarios. Hence, the ESCC OPCM stands out as a more advantageous choice compared to chemical-induced models (which fail to generate tumors with well-defined genetic characteristics),[31,32] patient-derived xenograft (PDX) models (which lack a specific driver mutation), or GEMMs(which require more laboratory materials and time).[33,34] Furthermore, the utilization of tumor organoids derived from OPCMs for large-scale compound screening has demonstrated their potential in supporting preclinical drug development efforts.

CellPress
OPEN ACCESS

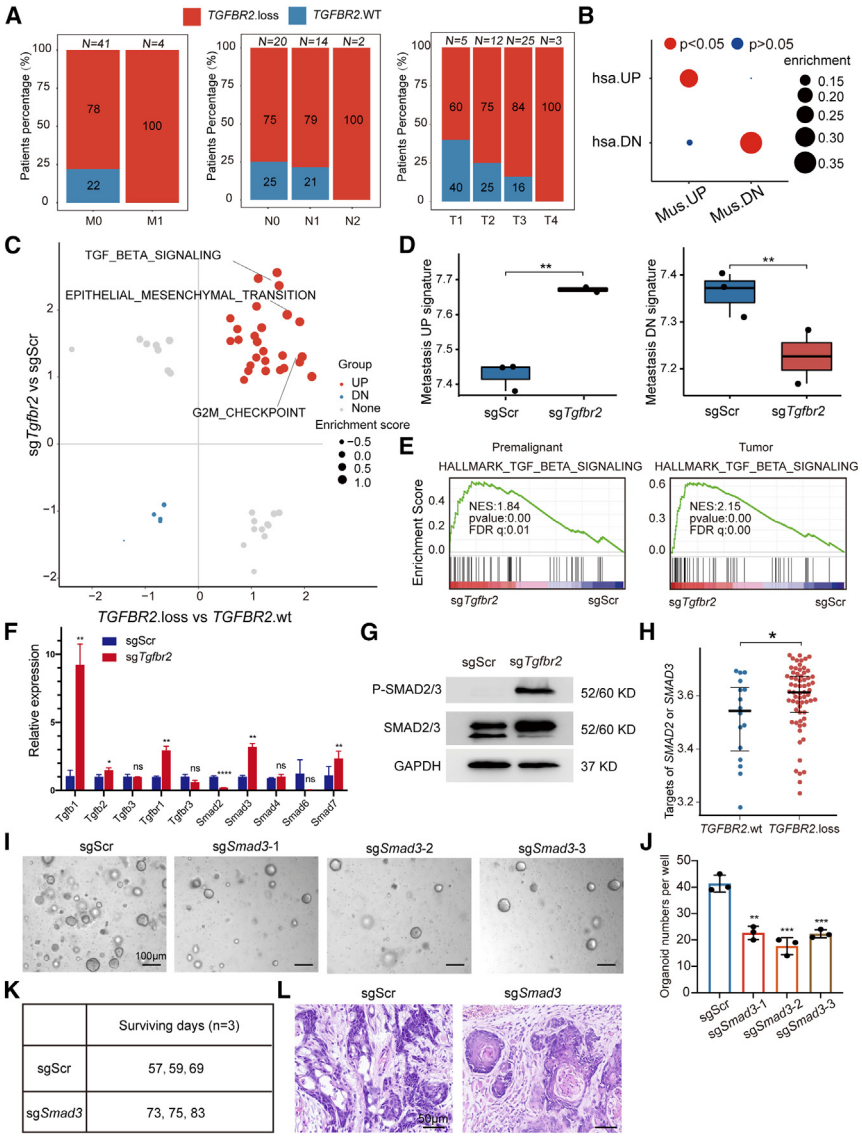

	Surviving days (n=3)
sgScr	57, 59, 69
sg*Smad3*	73, 75, 83

Figure 5. The molecular features of TGFBR2-deficient ESCC

(A) Bar plot of the proportion of *TGFBR2* loss in patients with ESCC from TCGA-ESCA database at different tumor stages according to TNM classification.

(B) The dot plot displaying the enrichment scores of murine TCMT tumor organoids versus TCM and patients with ESCC with *TGFBR2* loss versus WT from TCGA-ESCA cohorts. Statistic values were determined by hypergeometric test.

(C) The scatterplot showing GSEA of HALLMARK OF CANCER in patients with ESCC with *TGFBR2* loss versus WT and murine TCMT tumor organoids versus TCM.

(D) Boxplots showing the mRNA expression levels of patients with ESCC upregulated or downregulated metastasis gene signatures expressed in murine TCM ($n = 3$) and TCMT ($n = 2$) tumor organoids. Chi-squared test was performed to determine the significant level; $^*p < 0.05$ and $^{**}p < 0.01$.

(E) GSEA showing positive enrichments of the HALLMARK_TGF_BETA_SIGNALING signatures in murine TCMT premalignant and tumor organoids compared to TCM.

(F) Bar plot showing the RT-qPCR for mRNA analysis of some TGF-β signaling pathway component genes. Experiments were performed three times, and data are represented as means ± SD. $^*p < 0.05$, $^{**}p < 0.01$, and $^{****}p < 0.0001$, ns, no significant, unpaired t test.

(G) Western blot showing the increase of SMAD2/3 expression and phosphorylation after *Tgfbr2* knockout.

(H) The Beeswarm plot showing the expression level of G.KOINUMA_TARGETS_OF_ SMAD2_OR_ SMAD3 pathway gene signatures in patients with ESCC with *TGFBR2* loss or WT from the TCGA-ESCA cohort.

(I) Bright-field images showing the decrease in the number of organoids formed after *Smad3* knockout in TCMT tumors. Three independent sgRNAs were used in this experiment. Scale bar, 100 μm.

(J) Bar plot showing the decrease in organoids formed after *Smad3* knockout in TCMT tumor. Data are the mean of three technique repeats. $^{**}p < 0.01$ and $^{***}p < 0.001$, unpaired t test.

(K) Table showing the survival time of TCMT recipient mice with or without *Smad3* knockout, $n = 3$.

(L) H&E staining pictures of TCMT OPCMs with or without *Smad3* knockout. Scale bar, 50 μm.

By utilizing the TCM background genotype, we can encompass most genetic mutation profiles observed in patients with esophageal cancer, closely paralleling clinical scenarios. Furthermore, organoids with TCM genotype exhibit prolonged tumorigenesis, providing an optimal window for the selection of candidate driver genes. Moreover, mutations may act as drivers only during certain stages of cancer development.

With OPCMs, we identified seven drivers in ESCC. The FAT family (*Fat1*, *Fat2*, and *Fat4*) is associated with tumor suppression and planar cell polarity.[35] *Kmt2d* and *Ep300* are histone regulators. The tumor-suppressor effect of *Kmt2d*[36] and the dual effect of *Ep300*[37] have been illustrated in lung cancer. *Notch2*, a crucial member of the NOTCH receptor family, plays a significant role in organ development.[38] The activation of NOTCH in lung adenocarcinoma, breast cancer, ovarian cancer, hepatocellular cancer, and colorectal cancer was determined to be oncogenic.[39] However, in other tumors, such as squamous cell carcinoma (SCC) and neuroendocrine tumors, it can also act as a tumor suppressor.[40] Research on the role of these genes in esophageal cancer has been poorly reported.

Notably, OPCM screening assays revealed that tumors with *Tgfbr2* knockout exhibited heightened aggressiveness and a propensity for metastasis. Consistent with ESCC, TGFBR2 deficiency also caused lung squamous cancer,[41,42] metastatic intestinal cancer,[43] pancreatic ductal adenocarcinoma,[44] cholangiocarcinoma,[45] breast cancer,[46] intraepithelial neoplasia in the prostate, and the development of invasive SCC in the forestomach.[47] These observations suggest that

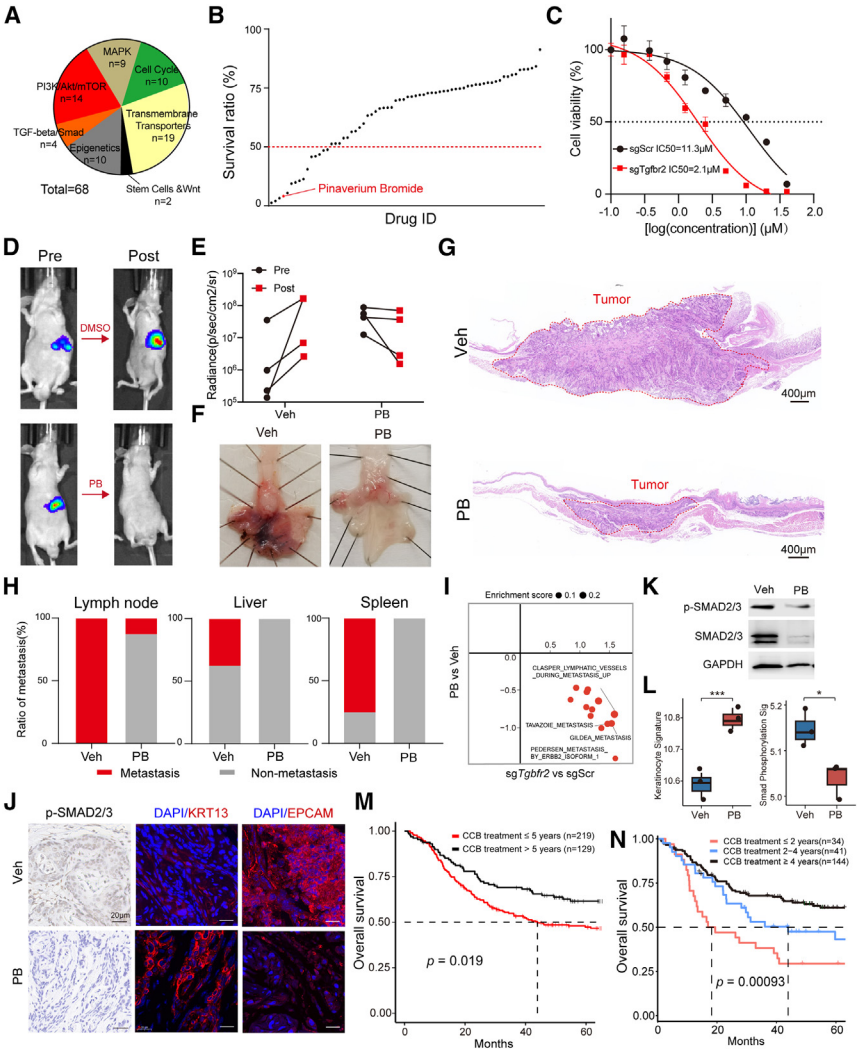

Figure 6. Drug screening with tumor organoids identified CCBs as a potential treatment for ESCC with TGFBR2 loss

(A) Pie chart shows the constitution of drug screening assay (total: 68 candidates, MAPK $n = 9$, cell Cycle $n = 10$, Pi3k/Akt/mTOR $n = 14$, TGF-β/Smad $n = 4$, epigenetics $n = 10$, stem cells and Wnt $n = 2$, and transmembrane transporters $n = 19$).

(B) Scatterplot showing the response of 65 drugs from the FDA drug library of TCMT tumor organoids. Pinaverium bromide (PB) is labeled in red.

(C) Drug dose-response curves of TCMT tumors and WT organoids treated with PB. Each point indicates the mean value of three replicates.

(D) Living images of recipient mice in vehicle and PB treatment groups, $n = 3$.

(E) Relative bioluminescence signal of pre- and post-treatment recipient mice in vehicle and PB treatment groups, $n = 4$.

(F) Bright-field images of pre- and post-treatment recipient mice in vehicle and PB treatment groups.

(G) H&E staining landscape pictures showing the decrease of tumor invasion area after PB treatment. Scale bar, 400 μm.

(H) Bar plots showing the percentage of lymph node, liver, and spleen metastasis under pre- and post-treatment, $n = 8$.

(I) Scatterplot showing the enrichment of metastasis-related pathways from TCMT versus TCM and PB versus vehicle-treated TCMT tumor organoids by GSEA.

(J) Immunohistochemical and immunofluorescence images of p-SMAD2/3 (left), KRT13 (middle), and EPCAM (right) in TCMT tumor tissue after vehicle or PB treatment.

(K) Western blot showing the decrease of p-SMAD2/3 protein level after 2 μM PB treatment *in vitro* in sg*Tgfbr2* tumor organoids.

(L) Boxplot showing mRNA expression level of PID_ECADHERIN_KERATINOCYTE_PATHWAY (left) and GO_POSITIVE_REGULATION_OF_PATHWAY_RESTRICTED_SMAD_PROTEIN_PHOSPHORYLATION (right) signature in PB- ($n = 3$) and vehicle-treated ($n = 3$) TCMT tumor organoids.

(M) The Kaplan-Meier survival curves of patients with ESCC from West China Hospital with calcium channel blocker (CCB) treatment for more than 5 or less than 5 years. The p value was calculated by log rank test.

(N) The Kaplan-Meier survival curves of patients with ESCC from West China Hospital with CCB treatment for $\leq$2 years, 2–4 years, and $\geq$4 years. The p value was calculated by log rank test.

TGFBR2/TGF-β signaling exerts a tumor-suppressive effect in fibroblasts and epithelial cells. In our study, several genes associated with this pathway were significantly upregulated in TGFBR2-deficient tumor cells, including the *Tgfb1* ligand, *Tgfbr1* receptor, and *Smad3* effector. The upregulation of *Tgfb1* and *Tgfbr1* is considered to be a negative feedback mechanism, which needs further verification. TGF-β has a biphasic role, functioning as both a tumor suppressor in premalignant cells and a tumor promoter in the late stages. These tumor cells have escaped canonical TGF-β-SMAD-signaling-induced growth inhibitory and apoptotic responses but retained or gained certain other responses to TGF-β stimulation.[48] In particular, it has been demonstrated that Erk/MAPK[49] and JNK/MAPK mediate the phosphorylation process of SMAD3.[50] Consistently, we observed activation of the MAPK pathway and an increased protein level of SMAD3 in TGFBR2-deficient tumor cells. However, the kinase responsible is not clear, and more experiments and data are needed to prove it directly. The pro-tumorigenic functions of SMAD3 have also been reported in other tumors.[51–54] Understanding the downstream effects of abrogation of TGF-β signaling in tumor cells may identify processes that can be targeted therapeutically. In this study, we found that the utilization of PB demonstrated effective and specific cytotoxicity to *TGFBR2*-deficient tumor cells, concurrent with the downregulation of SMAD3 protein levels and facilitation of tumor differentiation (Figure 6). It has been reported that reduction in the Ca^{2+}-dependent differentiation pathway emerges as a pivotal factor in the malignant transformation of ESCC,[55] underscoring the critical role of the calcium signaling pathway in this context. However, there is limited research on this class of drugs in esophageal

cancer. In the clinic, patients with ESCC subjected to CCB therapy for a duration exceeding 5 years had a better prognosis, making them a novel target for potential clinical applications.

Limitations of the study

In this study, we revealed the roles of *Tgfbr2* loss in the development and progression of ESCC. While we showed that *Smad3* was activated in *Tgfbr2*-deficient tumors, the molecular mechanism underlying its activation remains unclear. Moreover, we found that *Tgfbr2*-deficient tumors could be restrained by PB, which also reduced the levels of p-SMAD3. However, the molecular link between calcium channels, potential targets of PB, and *Smad3* needs to be further studied.

RESOURCE AVAILABILITY

Lead contact

Further information and requests for resources and reagents should be directed to and will be fulfilled by the lead contact, Chong Chen (chongchen@scu.edu.cn).

Materials availability

All unique reagents generated in this study are available from the lead contact with a completed materials transfer agreement.

Data and code availability

- The bulk RNA-seq data have been deposited in the NCBI Gene Expression Omnibus database with accession number GEO: GSE249583. The accession numbers for the datasets are listed in the key resources table.
- This paper does not report original code.
- Any additional information required to reanalyze the data reported in this work paper is available from the lead contact upon request.

ACKNOWLEDGMENTS

We thank the Chen-Liu lab members for discussions and technical support; the Department of Gastroenterology and the Department of Thoracic Surgery for their clinical resources; Professor Deying Kang of statistics (West China Hospital, Sichuan University, China) for the constructive suggestions on the clinical survival analysis; the Core Facilities of West China Hospital, Sichuan University, and the Chengdu Organoid Med Medical Laboratory for technical support; and Fangfang Wang (Institute of Hematology, West China Hospital) and Shasha Du for the graphical abstract artwork. This study was supported by the National Natural Science Foundation of China (82330087, T2221004, 82130007, 82170171, 82472783, 82000514, 82170675, and 82303317); the Frontiers Medical Center, Tianfu Jincheng Laboratory Foundation (TFJC2023010004); the 1.3.5. Project for Disciplines of Excellence, West China Hospital, Sichuan University (ZYJC21003, ZYGD22012, and ZYJC21011); the Sichuan Science and Technology Program (2023ZYD0057 and 2023NSFSC1904); the National Clinical Research Center for Geriatrics, West China Hospital, Sichuan University (Z2024JC001); the Basic Research Projects of Qinghai Provincial Department of Science and Technology (2023-ZJ-791); the China Postdoctoral Science Foundation (2023M732434 and 2023M732457); the Sichuan Province Innovative Talent Funding Project for Postdoctoral Fellows; and the Postdoctoral Fellowship Program of CPSF (GZB20230466).

AUTHOR CONTRIBUTIONS

Conceptualization, C.C.; methodology, J.W., J.D., Y.Z., Z.L., X.W., L.W., H. Liu, S.D., S.Z., X.X., P.T., M.W., B.W., Q.Z., Y.W., M.Z., R.L., H. Lin, Yuan Li, Yaxin Li, and Z.H.; bioinformatic analysis, X.L., X.P., X.C., and A.Z.; clinic resources, L.G., Yixin Liu, and J.Z.; writing – original draft, J.W., J.D., and X.L.; writing – review & editing, C.C.; funding acquisition, L.G., F.N., and C.C.; supervision, L.C., B.H., Yu Liu, F.N., and C.C.

DECLARATION OF INTERESTS

A patent (no. 202010684524.2) for the primary *in situ* mouse model of esophagus based on organoids has been applied for by West China Hospital, Sichuan University.

STAR★METHODS

Detailed methods are provided in the online version of this paper and include the following:

- KEY RESOURCES TABLE
- EXPERIMENTAL MODELS AND SUBJECTS DETAILS
- METHOD DETAILS
  - Plasmids and transduction
  - Organoid culture
  - Genomic DNA extraction, PCR amplification
  - Establishment of an orthotopic esophageal carcinoma mouse model
  - Bioluminescent imaging
  - Quantitative Real-Time PCR
  - Western blotting
  - H&E, immunohistochemistry, and immunofluorescence staining
  - Drug treatment
  - RNA-seq analyses
  - Clinical correlation analyses
  - Gene signatures identification
  - Survival analyses
- QUANTIFICATION AND STATISTICAL ANALYSIS

SUPPLEMENTAL INFORMATION

Supplemental information can be found online at https://doi.org/10.1016/j.celrep.2024.114952.

Received: March 11, 2024
Revised: August 31, 2024
Accepted: October 18, 2024
Published: November 10, 2024

REFERENCES

1. Sawada, G., Niida, A., Uchi, R., Hirata, H., Shimamura, T., Suzuki, Y., Shiraishi, Y., Chiba, K., Imoto, S., Takahashi, Y., et al. (2016). Genomic Landscape of Esophageal Squamous Cell Carcinoma in a Japanese Population. Gastroenterology *150*, 1171–1182. https://doi.org/10.1053/j.gastro.2016.01.035.
2. Pennathur, A., Gibson, M.K., Jobe, B.A., and Luketich, J.D. (2013). Oesophageal carcinoma. Lancet *381*, 400–412. https://doi.org/10.1016/S0140-6736(12)60643-6.
3. Gao, Y.B., Chen, Z.L., Li, J.G., Hu, X.D., Shi, X.J., Sun, Z.M., Zhang, F., Zhao, Z.R., Li, Z.T., Liu, Z.Y., et al. (2014). Genetic landscape of esophageal squamous cell carcinoma. Nat. Genet. *46*, 1097–1102. https://doi.org/10.1038/ng.3076.
4. Cancer Genome Atlas Research Network; Analysis Working Group Asan University; BC Cancer Agency; Brigham and Women's Hospital; Broad Institute; Brown University; Case Western Reserve University; Dana-Farber Cancer Institute; Duke University; Greater Poland Cancer Centre (2017). Integrated genomic characterization of oesophageal carcinoma. Nature *541*, 169–175. https://doi.org/10.1038/nature20805.
5. Cheng, C., Zhou, Y., Li, H., Xiong, T., Li, S., Bi, Y., Kong, P., Wang, F., Cui, H., Li, Y., et al. (2016). Whole-Genome Sequencing Reveals Diverse Models of Structural Variations in Esophageal Squamous Cell Carcinoma. Am. J. Hum. Genet. *98*, 256–274. https://doi.org/10.1016/j.ajhg.2015.12.013.

6. Cui, Y., Chen, H., Xi, R., Cui, H., Zhao, Y., Xu, E., Yan, T., Lu, X., Huang, F., Kong, P., et al. (2020). Whole-genome sequencing of 508 patients identifies key molecular features associated with poor prognosis in esophageal squamous cell carcinoma. Cell Res. *30*, 902–913. https://doi.org/10.1038/s41422-020-0333-6.
7. Agrawal, N., Jiao, Y., Bettegowda, C., Hutfless, S.M., Wang, Y., David, S., Cheng, Y., Twaddell, W.S., Latt, N.L., Shin, E.J., et al. (2012). Comparative genomic analysis of esophageal adenocarcinoma and squamous cell carcinoma. Cancer Discov. *2*, 899–905. https://doi.org/10.1158/2159-8290.CD-12-0189.
8. Lin, D.C., Hao, J.J., Nagata, Y., Xu, L., Shang, L., Meng, X., Sato, Y., Okuno, Y., Varela, A.M., Ding, L.W., et al. (2014). Genomic and molecular characterization of esophageal squamous cell carcinoma. Nat. Genet. *46*, 467–473. https://doi.org/10.1038/ng.2935.
9. Martincorena, I., Fowler, J.C., Wabik, A., Lawson, A.R.J., Abascal, F., Hall, M.W.J., Cagan, A., Murai, K., Mahbubani, K., Stratton, M.R., et al. (2018). Somatic mutant clones colonize the human esophagus with age. Science *362*, 911–917. https://doi.org/10.1126/science.aau3879.
10. Colom, B., Alcolea, M.P., Piedrafita, G., Hall, M.W.J., Wabik, A., Dentro, S.C., Fowler, J.C., Herms, A., King, C., Ong, S.H., et al. (2020). Spatial competition shapes the dynamic mutational landscape of normal esophageal epithelium. Nat. Genet. *52*, 604–614. https://doi.org/10.1038/s41588-020-0624-3.
11. Nakayama, M., Hong, C.P., Oshima, H., Sakai, E., Kim, S.J., and Oshima, M. (2020). Loss of wild-type p53 promotes mutant p53-driven metastasis through acquisition of survival and tumor-initiating properties. Nat. Commun. *11*, 2333. https://doi.org/10.1038/s41467-020-16245-1.
12. Abby, E., Dentro, S.C., Hall, M.W.J., Fowler, J.C., Ong, S.H., Sood, R., Herms, A., Piedrafita, G., Abnizova, I., Siebel, C.W., et al. (2023). Notch1 mutations drive clonal expansion in normal esophageal epithelium but impair tumor growth. Nat. Genet. *55*, 232–245. https://doi.org/10.1038/s41588-022-01280-z.
13. Mahmoudian, R.A., Farshchian, M., and Abbaszadegan, M.R. (2021). Genetically engineered mouse models of esophageal cancer. Exp. Cell Res. *406*, 112757. https://doi.org/10.1016/j.yexcr.2021.112757.
14. Opitz, O.G., Harada, H., Suliman, Y., Rhoades, B., Sharpless, N.E., Kent, R., Kopelovich, L., Nakagawa, H., and Rustgi, A.K. (2002). A mouse model of human oral-esophageal cancer. J. Clin. Invest. *110*, 761–769. https://doi.org/10.1172/JCI15324.
15. Na, F., Pan, X., Chen, J., Chen, X., Wang, M., Chi, P., You, L., Zhang, L., Zhong, A., Zhao, L., et al. (2022). KMT2C deficiency promotes small cell lung cancer metastasis through DNMT3A-mediated epigenetic reprogramming. Nat. Cancer *3*, 753–767. https://doi.org/10.1038/s43018-022-00361-6.
16. Lu, Z., Zhong, A., Liu, H., Zhang, M., Chen, X., Pan, X., Wang, M., Deng, X., Gao, L., Zhao, L., et al. (2022). Dissecting the genetic and microenvironmental factors of gastric tumorigenesis in mice. Cell Rep. *41*, 111482. https://doi.org/10.1016/j.celrep.2022.111482.
17. Drost, J., van Jaarsveld, R.H., Ponsioen, B., Zimberlin, C., van Boxtel, R., Buijs, A., Sachs, N., Overmeer, R.M., Offerhaus, G.J., Begthel, H., et al. (2015). Sequential cancer mutations in cultured human intestinal stem cells. Nature *521*, 43–47. https://doi.org/10.1038/nature14415.
18. Chen, J., Dai, S., Zhao, L., Peng, Y., Sun, C., Peng, H., Zhong, Q., Quan, Y., Li, Y., Chen, X., et al. (2023). A New Type of Endometrial Cancer Models in Mice Revealing the Functional Roles of Genetic Drivers and Exploring their Susceptibilities. Adv. Sci. *10*, e2300383. https://doi.org/10.1002/advs.202300383.
19. Kandiah, K., Chedgy, F.J.Q., Subramaniam, S., Thayalasekaran, S., Kurup, A., and Bhandari, P. (2017). Early squamous neoplasia of the esophagus: The endoscopic approach to diagnosis and management. Saudi J. Gastroenterol. *23*, 75–81. https://doi.org/10.4103/1319-3767.203366.
20. Ohashi, S., Miyamoto, S., Kikuchi, O., Goto, T., Amanuma, Y., and Muto, M. (2015). Recent Advances From Basic and Clinical Studies of Esophageal Squamous Cell Carcinoma. Gastroenterology *149*, 1700–1715. https://doi.org/10.1053/j.gastro.2015.08.054.
21. Que, J., Okubo, T., Goldenring, J.R., Nam, K.T., Kurotani, R., Morrisey, E.E., Taranova, O., Pevny, L.H., and Hogan, B.L.M. (2007). Multiple dose-dependent roles for Sox2 in the patterning and differentiation of anterior foregut endoderm. Development *134*, 2521–2531. https://doi.org/10.1242/dev.003855.
22. Taylor, A.M., Shih, J., Ha, G., Gao, G.F., Zhang, X., Berger, A.C., Schumacher, S.E., Wang, C., Hu, H., Liu, J., et al. (2018). Genomic and Functional Approaches to Understanding Cancer Aneuploidy. Cancer Cell *33*, 676–689.e3. https://doi.org/10.1016/j.ccell.2018.03.007.
23. Liberzon, A., Birger, C., Thorvaldsdóttir, H., Ghandi, M., Mesirov, J.P., and Tamayo, P. (2015). The Molecular Signatures Database (MSigDB) hallmark gene set collection. Cell Syst. *1*, 417–425. https://doi.org/10.1016/j.cels.2015.12.004.
24. Massague, J. (2012). TGFbeta signalling in context. Nat. Rev. Mol. Cell Biol. *13*, 616–630. https://doi.org/10.1038/nrm3434.
25. Driehuis, E., Kretzschmar, K., and Clevers, H. (2020). Establishment of patient-derived cancer organoids for drug-screening applications. Nat. Protoc. *15*, 3380–3409. https://doi.org/10.1038/s41596-020-0379-4.
26. Lo, Y.H., Kolahi, K.S., Du, Y., Chang, C.Y., Krokhotin, A., Nair, A., Sobba, W.D., Karlsson, K., Jones, S.J., Longacre, T.A., et al. (2021). A CRISPR/Cas9-Engineered ARID1A-Deficient Human Gastric Cancer Organoid Model Reveals Essential and Nonessential Modes of Oncogenic Transformation. Cancer Discov. *11*, 1562–1581. https://doi.org/10.1158/2159-8290.CD-20-1109.
27. Wang, M., Chen, X., Tan, P., Wang, Y., Pan, X., Lin, T., Jiang, Y., Wang, B., Xu, H., Wang, Y., et al. (2022). Acquired semi-squamatization during chemotherapy suggests differentiation as a therapeutic strategy for bladder cancer. Cancer Cell *40*, 1044–1059.e8. https://doi.org/10.1016/j.ccell.2022.08.010.
28. Zhao, H., Cheng, Y., Kalra, A., Ma, K., Zheng, Y., Ziman, B., Tressler, C., Glunde, K., Shin, E.J., Ngamruengphong, S., et al. (2022). Generation and multiomic profiling of a TP53/CDKN2A double-knockout gastroesophageal junction organoid model. Sci. Transl. Med. *14*, eabq6146. https://doi.org/10.1126/scitranslmed.abq6146.
29. Ko, K.P., Huang, Y., Zhang, S., Zou, G., Kim, B., Zhang, J., Jun, S., Martin, C., Dunbar, K.J., Efe, G., et al. (2023). Key Genetic Determinants Driving Esophageal Squamous Cell Carcinoma Initiation and Immune Evasion. Gastroenterology *165*, 613–628.e20. https://doi.org/10.1053/j.gastro.2023.05.030.
30. Wu, Z., Zhou, J., Zhang, X., Zhang, Z., Xie, Y., Liu, J.B., Ho, Z.V., Panda, A., Qiu, X., Cejas, P., et al. (2021). Reprogramming of the esophageal squamous carcinoma epigenome by SOX2 promotes ADAR1 dependence. Nat. Genet. *53*, 881–894. https://doi.org/10.1038/s41588-021-00859-2.
31. Quante, M., Bhagat, G., Abrams, J.A., Marache, F., Good, P., Lee, M.D., Lee, Y., Friedman, R., Asfaha, S., Dubeykovskaya, Z., et al. (2012). Bile acid and inflammation activate gastric cardia stem cells in a mouse model of Barrett-like metaplasia. Cancer Cell *21*, 36–51. https://doi.org/10.1016/j.ccr.2011.12.004.
32. Tang, X.H., Knudsen, B., Bemis, D., Tickoo, S., and Gudas, L.J. (2004). Oral cavity and esophageal carcinogenesis modeled in carcinogen-treated mice. Clin. Cancer Res. *10*, 301–313. https://doi.org/10.1158/1078-0432.ccr-0999-3.
33. Tetreault, M.P., Wang, M.L., Yang, Y., Travis, J., Yu, Q.C., Klein-Szanto, A.J., and Katz, J.P. (2010). Klf4 overexpression activates epithelial cytokines and inflammation-mediated esophageal squamous cell cancer in mice. Gastroenterology *139*, 2124–2134.e9. https://doi.org/10.1053/j.gastro.2010.08.048.
34. Tetreault, M.P., Yang, Y., Travis, J., Yu, Q.C., Klein-Szanto, A., Tobias, J.W., and Katz, J.P. (2010). Esophageal squamous cell dysplasia and delayed differentiation with deletion of kruppel-like factor 4 in murine esophagus. Gastroenterology *139*, 171–181.e9. https://doi.org/10.1053/j.gastro.2010.03.048.

35. Katoh, M. (2012). Function and cancer genomics of FAT family genes (review). Int. J. Oncol. *41*, 1913–1918. https://doi.org/10.3892/ijo.2012.1669.

36. Pan, Y., Han, H., Hu, H., Wang, H., Song, Y., Hao, Y., Tong, X., Patel, A.S., Misirlioglu, S., Tang, S., et al. (2023). KMT2D deficiency drives lung squamous cell carcinoma and hypersensitivity to RTK-RAS inhibition. Cancer Cell *41*, 88–105.e8. https://doi.org/10.1016/j.ccell.2022.11.015.

37. Kim, K.B., Kabra, A., Kim, D.W., Xue, Y., Huang, Y., Hou, P.C., Zhou, Y., Miranda, L.J., Park, J.I., Shi, X., et al. (2022). KIX domain determines a selective tumor-promoting role for EP300 and its vulnerability in small cell lung cancer. Sci. Adv. *8*, eabl4618. https://doi.org/10.1126/sciadv.abl4618.

38. Zhou, B., Lin, W., Long, Y., Yang, Y., Zhang, H., Wu, K., and Chu, Q. (2022). Notch signaling pathway: architecture, disease, and therapeutics. Signal Transduct. Target. Ther. *7*, 95. https://doi.org/10.1038/s41392-022-00934-y.

39. Aster, J.C., Pear, W.S., and Blacklow, S.C. (2017). The Varied Roles of Notch in Cancer. Annu. Rev. Pathol. *12*, 245–275. https://doi.org/10.1146/annurev-pathol-052016-100127.

40. Nowell, C.S., and Radtke, F. (2017). Notch as a tumour suppressor. Nat. Rev. Cancer *17*, 145–159. https://doi.org/10.1038/nrc.2016.145.

41. Dhainaut, M., Rose, S.A., Akturk, G., Wroblewska, A., Nielsen, S.R., Park, E.S., Buckup, M., Roudko, V., Pia, L., Sweeney, R., et al. (2022). Spatial CRISPR genomics identifies regulators of the tumor microenvironment. Cell *185*, 1223–1239.e20. https://doi.org/10.1016/j.cell.2022.02.015.

42. Wang, Y., Tan, X., Tang, Y., Zhang, C., Xu, J., Zhou, J., Cheng, X., Hou, N., Liu, W., Yang, G., et al. (2019). Dysregulated Tgfbr2/ERK-Smad4/SOX2 Signaling Promotes Lung Squamous Cell Carcinoma Formation. Cancer Res. *79*, 4466–4479. https://doi.org/10.1158/0008-5472.CAN-19-0161.

43. Sakai, E., Nakayama, M., Oshima, H., Kouyama, Y., Niida, A., Fujii, S., Ochiai, A., Nakayama, K.I., Mimori, K., Suzuki, Y., et al. (2018). Combined Mutation of Apc, Kras, and Tgfbr2 Effectively Drives Metastasis of Intestinal Cancer. Cancer Res. *78*, 1334–1346. https://doi.org/10.1158/0008-5472.CAN-17-3303.

44. Mueller, S., Engleitner, T., Maresch, R., Zukowska, M., Lange, S., Kaltenbacher, T., Konukiewitz, B., Öllinger, R., Zwiebel, M., Strong, A., et al. (2018). Evolutionary routes and KRAS dosage define pancreatic cancer phenotypes. Nature *554*, 62–68. https://doi.org/10.1038/nature25459.

45. Morris, S.M., Carter, K.T., Baek, J.Y., Koszarek, A., Yeh, M.M., Knoblaugh, S.E., and Grady, W.M. (2015). TGF-beta signaling alters the pattern of liver tumorigenesis induced by Pten inactivation. Oncogene *34*, 3273–3282. https://doi.org/10.1038/onc.2014.258.

46. Bierie, B., Stover, D.G., Abel, T.W., Chytil, A., Gorska, A.E., Aakre, M., Forrester, E., Yang, L., Wagner, K.U., and Moses, H.L. (2008). Transforming growth factor-beta regulates mammary carcinoma cell survival and interaction with the adjacent microenvironment. Cancer Res. *68*, 1809–1819.

47. Bhowmick, N.A., Chytil, A., Plieth, D., Gorska, A.E., Dumont, N., Shappell, S., Washington, M.K., Neilson, E.G., and Moses, H.L. (2004). TGF-beta signaling in fibroblasts modulates the oncogenic potential of adjacent epithelia. Science *303*, 848–851. https://doi.org/10.1126/science.1090922.

48. David, C.J., and Massague, J. (2018). Contextual determinants of TGFbeta action in development, immunity and cancer. Nat. Rev. Mol. Cell Biol. *19*, 419–435. https://doi.org/10.1038/s41580-018-0007-0.

49. Kretzschmar, M., Doody, J., Timokhina, I., and Massagué, J. (1999). A mechanism of repression of TGFbeta/Smad signaling by oncogenic Ras. Genes Dev. *13*, 804–816. https://doi.org/10.1101/gad.13.7.804.

50. Engel, M.E., McDonnell, M.A., Law, B.K., and Moses, H.L. (1999). Interdependent SMAD and JNK signaling in transforming growth factor-beta-mediated transcription. J. Biol. Chem. *274*, 37413–37420. https://doi.org/10.1074/jbc.274.52.37413.

51. Tang, P.M.K., Zhou, S., Meng, X.M., Wang, Q.M., Li, C.J., Lian, G.Y., Huang, X.R., Tang, Y.J., Guan, X.Y., Yan, B.P.Y., et al. (2017). Smad3 promotes cancer progression by inhibiting E4BP4-mediated NK cell development. Nat. Commun. *8*, 14677. https://doi.org/10.1038/ncomms14677.

52. Blum, A.E., Venkitachalam, S., Ravillah, D., Chelluboyina, A.K., Kieber-Emmons, A.M., Ravi, L., Kresak, A., Chandar, A.K., Markowitz, S.D., Canto, M.I., et al. (2019). Systems Biology Analyses Show Hyperactivation of Transforming Growth Factor-beta and JNK Signaling Pathways in Esophageal Cancer. Gastroenterology *156*, 1761–1774. https://doi.org/10.1053/j.gastro.2019.01.263.

53. Morris, S.M., Baek, J.Y., Koszarek, A., Kanngurn, S., Knoblaugh, S.E., and Grady, W.M. (2012). Transforming growth factor-beta signaling promotes hepatocarcinogenesis induced by p53 loss. Hepatology *55*, 121–131. https://doi.org/10.1002/hep.24653.

54. Zhang, L., Zhu, Z., Yan, H., Wang, W., Wu, Z., Zhang, F., Zhang, Q., Shi, G., Du, J., Cai, H., et al. (2021). Creatine promotes cancer metastasis through activation of Smad2/3. Cell Metab. *33*, 1111–1123.e4. https://doi.org/10.1016/j.cmet.2021.03.009.

55. Luo, A., Kong, J., Hu, G., Liew, C.C., Xiong, M., Wang, X., Ji, J., Wang, T., Zhi, H., Wu, M., and Liu, Z. (2004). Discovery of Ca2+-relevant and differentiation-associated genes downregulated in esophageal squamous cell carcinoma using cDNA microarray. Oncogene *23*, 1291–1299. https://doi.org/10.1038/sj.onc.1207218.

56. Love, M.I., Huber, W., and Anders, S. (2014). Moderated estimation of fold change and dispersion for RNA-seq data with DESeq2. Genome Biol. *15*, 550. https://doi.org/10.1186/s13059-014-0550-8.

57. Subramanian, A., Tamayo, P., Mootha, V.K., Mukherjee, S., Ebert, B.L., Gillette, M.A., Paulovich, A., Pomeroy, S.L., Golub, T.R., Lander, E.S., and Mesirov, J.P. (2005). Gene set enrichment analysis: a knowledge-based approach for interpreting genome-wide expression profiles. Proc. Natl. Acad. Sci. USA *102*, 15545–15550. https://doi.org/10.1073/pnas.0506580102.

58. Schneider, C.A., Rasband, W.S., and Eliceiri, K.W. (2012). NIH Image to ImageJ: 25 years of image analysis. Nat. Methods *9*, 671–675. https://doi.org/10.1038/nmeth.2089.

STAR★METHODS

KEY RESOURCES TABLE

REAGENT or RESOURCE	SOURCE	IDENTIFIER
Antibodies		
Anti-P40	Abcam	Cat# ab203826; RRID: AB_2934266
Anti- Cytokeratin5	RTM BIO	Cat# PTM-5040;
Anti- Cytokeratin14	RTM BIO	Cat# PTM-5391
Anti- Cytokeratin13	NOVUS	Cat# NBP1-97797
Anti- Cytokeratin7	Abcam	Cat# ab181598; RRID: AB_2783822
Anti-Ki67	Abcam	Cat# ab15580; RRID: AB_443209
Anti-CRISPR-Cas9 SP [JM11-55]	HUABIO	Cat# ET1703-85; RRID: AB_3070439
Anti-GAPDH	Cell Signaling Technology	Cat# 92310SF
Anti-TGFBR2	Abcam	Cat# ab283230
Anti- SMAD2/3	Abcam	Cat# ab202445
Anti-Phospho-SMAD2-S465/S467+ SMAD3-S423/S425	arigo	Cat# ARG40897
Anti- SMAD2	BOSTER	Cat# BM3992
Anti- SMAD3	BOSTER	Cat# BM3919
Anti-*c*-Myc (phospho S62) antibody [EPR17924]	Abcam	Cat# ab185656; RRID: AB_2935659
Bacterial and virus strains		
DH5a		TSV-A07
Biological samples		
Mouse sample	This paper	N/A
Chemicals, peptides, and recombinant proteins		
DPBS	GIBCO	Cat# C14190500BT
DMED/F12(1:1) basic(1X)	GIBCO	Cat# C11330500BT
DMEM	GIBCO	Cat# C11995500BT
Penicillin/Streptomycin	GIBCO	Cat# 15140-122
TrypLE™	GIBCO	Cat# 12604-028
Trypsin	GIBCO	Cat# 25200-072
GlutaMAX	GIBCO	Cat# 35050-061
B27	GIBCO	Cat# A3582801
N2	GIBCO	Cat# 17502048
N-acetylcysteine	Sigma	Cat# A9165
Nicotinamide	Sigma	Cat# N0636
EGF	Peprotech	Cat# AF-100-15-1000
Noggin	Peprotech	Cat# 120-10C-250
FGF10	Peprotech	Cat# 100-26-1000
R-spondin-1	Peprotech	Cat# 120-38-1000
A83-01	Peprotech	Cat# 9094360
T7E1 enzyme	Vazyme	Cat# EN303-01
Protein kinase K	Solarbio	Cat# P9460
D-luciferin potassium salt	Biovision	Cat# 7903-10PK
Matrigel	Corning	Cat# 356237
Protease inhibitors	Beyotime	Cat# P1045
TRIzol	Applied Biosystems	Cat# 15596026
SYBR	Applied Biosystems	Cat# A25741
FBS	HAKATA	Cat#HB-FBS-500

(*Continued on next page*)

Continued

REAGENT or RESOURCE	SOURCE	IDENTIFIER
DMSO	MPbio	Cat# 196055
Pinaverium bromide	Selleck	Cat# S6473
Calbryte™ 630 a.m.	AAT Bioquest	Cat# 20720
FDA-approved Drug Library	Selleck	Cat# L2000-Z398716
Deposited data		
Data files for Omics data (raw data of RNA-seq) of this paper	GEO	GSE249583
20 highly frequently altered genes of 323 ESCC samples	TCGA, ICGC and UCLA	https://www.cbioportal.org/
Experimental models: Cell lines		
Human: HEK-293T	ATCC	Cat# CRL-1573, RRID: CVCL_0045
Experimental models: Organisms/strains		
Mouse： CAG-Cas9-EGFP	The Jackson Lab	Cat# N0026179
Mouse：Trp53$^{-/-}$	The Jackson Lab	Cat# N0002101
Oligonucleotides		
CRISPR sgRNAs see Table S1A	DNA2.0	https://www.atum.bio/eCommerce/cas9/input
T7E1 assay PCR primer, see Table S1B	N/A	https://sg.idtdna.com/PrimerQuest/Home/Index
RT-qPCR primer, see Table S1C	N/A	https://sg.idtdna.com/PrimerQuest/Home/Index
Recombinant DNA		
psPAX2	Addgene	Cat# 12260
pMD2.G	Addgene	Cat# 12259
pCL-Eco	Addgene	Cat# 12371
pCAG-VSVG	Addgene	Cat# 35616
pLenti-U6-gRNA-EFS-mCherry	Na et al.[15]	N/A
pLenti-U6-sgCdkn2a-EFS-GFP	This paper	N/A
pMSCV-cMyc-iRES-luci2	Na et al.[15]	N/A
Software and algorithms		
DESeq2	Love et al.[56]	https://bioconductor.org/packages/release/bioc/html/DESeq2.html
Pheatmap	bioconductor	https://cran.rproject.org/web/packages/pheatmap
ggplot2	bioconductor	https://cran.r-project.org/package=ggplot2
GSEA	Subramanian et al.[57]	https://www.gseamsigdb.org/gsea/index.jsp
ImageJ	Schneider et al.[58]	https://imagej.nih.gov/ij/; RRID:SCR_003070
Survival	bioconductor	https://cran.rproject.org/web/packages/survival
Snapgene	Snapgene	https://www.snapgene.com
SPSS version 23.0	IBM Corp., Armonk, NY, USA	https://spss.en.softonic.com/mac?ex=RAMP-2081.3
Graphpad Prism 9	Graphpad Software	www.graphpad.com/scientifificsoftware/prism/

EXPERIMENTAL MODELS AND SUBJECTS DETAILS

C57BL/6 immunocompetent mice and BALB/c-Nude immunodeficient nude mice were purchased from Beijing HuaFukang Biological Technology Co. Ltd (6-8-week-old male). Trp53 knockout mouse (Jackson Lab, Cat# N0002101) and *Rosa26-CAG-Cas9-IRES-GFP* ((hereafter referred to as Cas9, Jackson Lab, Cat# N0026179) knock-in mice were purchased from the Jackson Laboratory. All mice used in this study were housed in animal facilities at the State Key Laboratory of Biotherapy of Sichuan University. The Institutional Animal Care approved all mice experiments and Use Committees of Sichuan University. Both the research team and the veterinary staff monitored animals once daily. Health was monitored by weight (twice weekly), food and water intake. The maximum size the tumors allowed to grow in the mice before euthanasia was 1000 mm^3.All recipient nude mice were randomly grouped before transplantation. In this study, n refers to number of mice. The testing order of each animal was randomized at each test day.

METHOD DETAILS

Plasmids and transduction

Full-length *Kras*^{G12D} and *Myc* cDNA were cloned into retroviral construct MSCV-cDNA-IRES-luciferase (Addgene, Cat# 18760), and guide RNAs were cloned into LentiCRISPRv2(U6-gRNA-EFS-mCherry, homemade). All plasmids were verified by sequencing. These resulting plasmids were transfected into HEK293T cells by calcium phosphate transfection method with the helper plasmids psPAX2 (Addgene, Cat# 12260), pMD2.G(Addgene, Cat# 12259) for sgRNAs vectors and pCL-Eco (Addgene, Cat# 12371), pCAG-VSVG (Addgene,# Cat# 1733) for overexpressing vectors. Collect the supernatant at 36h and 48h, the virus stock solution, and use it to transduce cell lines or organoids. Two days later,1 μg/ml puromycin (Gibco, Cat# A1113803) was added to select positive cells for several passages. Selected knockout clones' genomes were extracted for PCR reaction and then subjected to T7E1 enzyme detection. The mutation was finally verified by DNA sequencing. The sequence of sgRNAs is listed in Table S1A.

Organoid culture

Normal or malignant transformed esophagus tissue was prepared for organoid cultures. Isolate about 1.5 cm of esophageal tissue and wash it with a PBS buffer solution containing antibiotics about five times (Gibco, Cat# 15240096). Transfer the tissue to a new 15mL centrifuge tube and minced with fine scissors. Add 0.25% Trypsin-EDTA (GIBCO, Cat# 2152925) and incubate at 37°C for about 1 h, then add serum-containin DMEM medium to stop digestion. Filter the mixture through a 70-μm cell strainer (JET BIOFIL, Cat#CSS-013-070), centrifuge at 400 g for 5 min, discard the supernatant, resuspend the bottom cells with Matrigel (Corning, Cat# 354230) on ice. Add 30 μL of the mixture to each well of a 48-well plate and supplemented with 200 μL complete medium containing 1 x B27 (GIBCO, Cat# A3582801), 1 x N2 (GIBCO, Cat# 17502048), EGF (R&D, Cat# 236-EG-01M, final 50 ng/mL), FGF10 (Peprotech, Cat# 100-26-1000, final 200 ng/mL),Y27632 (Abmole Bioscience, Cat# No. M1817, final 10 μM), A83-01 (Peprotech, Cat# 9094360, final 2 μM), R-spodin 1 (Peprotech, Cat# 120-38-1000, final 250 ng/mL), Noggin (Peprotech, Cat# 120-10C-250, final 100 ng/mL), 10% Wnt-3A conditioned medium, Nicotinamide (Sigma, Cat #N0636, 1mM), N-acetylcysteine (Sigma, Cat# A9165, 1mM), Glutamax (Peprotech, Cat# 35050-061, 2 mM), and 1 x Penicillin/Streptomycin (GIBCO,Cat# 15140-122) in DMEM-F12 (GIBCO, Cat# 8121062). After 3–4 days, single cells can be observed growing into organoids, and timely passage can be performed. For maintenance, the established organoids were dissociated into single cells with TrypLE (GIBCO, Cat# 12605-028) and passaged at a 1:2 or 1:3 ratio.

Genomic DNA extraction, PCR amplification

Cells were collected, and 500 μL of DNA lysis buffer (Homemade, 10 mM Tris, 100 mM NaCl, 10mM EDTA, 0.5% SDS, 0.4 mg/mL proteinase K) was added and then incubated at 55°C for at least 2 h. The supernatant was combined with 500μL isopropanol, mixed, and centrifuged at 13,000 rpm for 10 min, remove the supernatant and then washed with 1mL75% ethanol once. Volatilized at 55°C for about 5 min, the DNA pellet was then dissolved in double-distilled water. 100 ng DNA was used for each genotyping PCR reaction. PCR reactions were performed on a ProFlex PCR system (Applied Biosystems). Primers used for PCR are shown in Table S1B.

Establishment of an orthotopic esophageal carcinoma mouse model

After passage and expansion to a sufficient number (2×10^5 cells per mouse), organoids were digested into single cells using TrypLE(Gibco, Cat# 12604021) described above and resuspended with a 20 μL 1:1 ratio of PBS and Matrigel, then placed on ice. After anesthetizing the recipient mice with isoflurane, a 0.5cm incision was made in their abdomen using surgical scissors; the esophagus was pulled out with forceps. The cell suspension was injected into the esophageal mucosa using an insulin needle; then, the incision was immediately sutured. Transplanted cell growth was monitored using a D-luciferin imaging system 20 days after transplantation, and imaging experiments were performed at different time points at the same intervals to record tumor progression. Several months later, the esophageal tumors were collected for pathological and related analyses based on the health status of the mice.

Bioluminescent imaging

After transplanted subcutaneously or orthotopically with organoids, mice would be periodically imaged to detect the luciferase fluorescence signal intensity with IVIS Spectrum (PerkinElmer) system. The mice were anesthetized with isoflurane after 250 μL 15 mg/ml D-luciferin, Potassium Salt (BioVision, Cat# 7903-1G) in PBS intraperitoneally injected.

Quantitative Real-Time PCR

Total RNAs were extracted by Trizol reagent (Invitrogen, Cat# 10296010) and phenol/chloroform methods. 2 μg total RNA was subject to reverse transcription using the HiScript II Q RT SuperMix for qPCR kit (Vazyme, Cat# R223-01) following the manufacturer's protocol. Gene expression was assayed by RT-qPCR on QuantStudio3 Real-Time PCR System (Applied Biosystems) using ChamQ Universal SYBR qPCR Master Mix (Vazyme, Cat# Q711-02/03). All reactions were repeated in three independent experiments with three technical repetitions for each sample. Primers used for qPCR analysis are shown in Table S1C.

Western blotting

Whole cell lysates were extracted in RIPA buffer (Beyotime, Cat# P0013) supplemented with protease inhibitors (Beyotime, Cat# P1045), followed by SDS–PAGE gel electrophoresis and blotting onto PVDF membranes. Primary antibodies were applied at 1:1000-1:5000 dilution in 5% non-fatty milk or BSA in TBST and incubated overnight at 4°C. HRP-conjugated secondary antibodies were applied at 1:10000 dilution. Images were developed by NcmECL Ultra Reagent (NCM biotech).

H&E, immunohistochemistry, and immunofluorescence staining

Tumor tissues were fixed with 4% PFA, embedded in paraffin, and cut into 5-μm-thick sections. For H&E staining, slices were stained with hematoxylin and eosin according to standard protocol. For immunohistochemistry, antigen retrieval was performed with 10 mM sodium citrate buffer after deparaffinization and rehydration. After permeabilization with 0.3% Triton X- and blocking with 2% goat serum, slices were incubated with primary antibodies at 4°C overnight. Horseradish peroxidase (HRP)-conjugated secondary antibodies (ZSGB-BIO, Cat# 2127A0609) were applied and incubated for 1 h at room temperature. Then, DAB (ZSGB-BIO, Cat# ZLI-9017) was applied to envision and hematoxylin for nuclear staining. The staining images were scanned with a panoramic MIDI (3DHISTECH).

Drug treatment

For the drug library screening, the 1000 single cells were cultured in a 96-well plate embedded in 5μL Matrigel, and organoids were treated with 10μM compound (Selleck, Cat# L2000-Z398716) (the drug list is shown in Table S2). For the Pinaverium bromide validation assay, 1000 single cells were cultured in a 96-well plate embedded in 5μL Matrigel and then subjected to different concentrations of Pinaverium bromide (Selleck, Cat# S6473) or DMSO. After 48h treatment, the number of organoids was counted in each view. The number of organoids in the experimental group normalized by the DMSO group was the cell viability. For drug treatment *in vivo* experiments, each mouse was injected intraperitoneally at 20 mg/kg every other day.

RNA-seq analyses

RNA was extracted from esophageal organoids with an integrity number (RIN) $\geq$ 7.5. RNA-seq libraries were prepared using the NEBNext Ultra RNA Library Prep Kit (NEB, Cat# E7770) for Illumina and were sequenced by the Illumina NovaSeq 6000 sequencing machine with 150-bp paired-end reads. The company removed adapter, poly-N, and low-quality reads of raw sequencing data for downstream analysis. Clean RNA-seq data were aligned to the mm10 reference using STAR_2.6.0a. Transcript abundances, significance levels, and differentially expressed genes were generated and identified by DESeq2. Genes with absolute fold changes >1 and p-value $\leq$0.05 were counted as differentially expressed. The significantly up-regulated genes in each group were used to perform KEGG enrichment analyses with the R package clusterProfiler (3.14.3). GSEA was utilized to identify the significantly enriched pathways by default parameters. Pheatmap was used to visualize differentially expressed genes with z scores. Nagpur (3.4.0) was used to portray the boxplot. P-values were calculated by t test. Venn diagrams were generated with the R package of Venerable (3.1.0.9000). All the transcriptome data in the boxplots were transformed by log2(X+1).

Clinical correlation analyses

The OncoPrint and cooperation between the highly frequently altered genes such as *TP53*, *MYC*, and *CDNK2A* in ESCC patients were analyzed using cBioPortal and demonstrated using Vennerable (v3.1.0.9000). The 20 highly frequently altered genes were analyzed in 3 cohorts (TCGA, ICGC and UCLA) from cBioPortal, comprising a total of 323 samples. *PIK3CA* shows gain and amplification; others show mutation, shallow deletion, and deep deletion. RNA-seq results and clinical data of ESCC patients were down loaded from the TCGA-ESCA cohort. Patients lacking paired omics and clinical data were excluded from this study.The frequency of *TGBFR2* loss, including mutations, shallow and deep deletion, was identified by cBioPortal reference.

Gene signatures identification

All transcriptome data in the TCGA database were log-transformed (log2(X+1)). The TNM stages refer to the AJCC clinical stage. ESCC patients were divided into T2/T3 andT1/T0, and the top 200 higher and lower expressed genes formed the tumor malignant UP and DN signatures, respectively. The correlation between *TGFBR2* expression levels and metastasis signatures, developed by the top 200 highly and lowly expressed genes in TCGA ESCC N1, N2 and N3 stages patients versus N0 stage patients, was calculated using Pearson's correlation coefficient. Statistic powers were quantified, followed by a two-sided hypothesis test with a confidence level of 0.95. GSEA was performed to elucidate the similarities of molecular features between ESCC patients and ESCC OPCMs. ESCC patients from TCGA were divided into *TGFBR2* loss and *TGFBR2* WT. The fold change of *TGFBR2* loss versus *TGFBR2* WT was used to obtain a rank-ordered gene list. The top 200 highly and lowly expressed genes in our model were saved as grp files.

Survival analyses

Information on all patients with esophageal squamous cell carcinoma was obtained from West China Hospital of Sichuan University. All 348 patients had a history of hypertension, and it was determined whether they were taking calcium channel inhibitors after follow-up. The Cox regression and the Kaplan-Meier survival curves were calculated and visualized by R package, survminer and survival. The characteristics of patients with and without calcium channel blocker (CCB) usage were compared using the chi-square test and

Fisher's exact test. Survival curves were calculated using the Kaplan-Meier method. The Cox proportional hazards regression model was utilized to analyze independent prognostic factors for overall survival through univariate and multivariate analyses. Clinically relevant factors with *p value* < 0.05 in the univariate analysis were included in the Cox regression multivariate analysis to identify independent prognostic factors for survival. Hazard ratios (HRs) and 95% confidence intervals (CIs) were generated, and *p value* < 0.05 was considered significant in the multivariate analysis. Statistical analysis was performed using SPSS version 23.0 software (IBM Corp., Armonk, NY, USA). Patient data used for statistics are shown in Tables S5 and S6.

QUANTIFICATION AND STATISTICAL ANALYSIS

Organoids diameters were measured by manually selecting well-focused organoids in images using ImageJ software. RT-qPCR, organoid diameter and number assays, tumor measurements, morphological statistics, and *in vitro* treatment were analyzed for statistical significance using two tailed unpaired parametric Student's t-tests (Prism 9.0, GraphPad software). Statistical test methods, sample sizes, and *p* values are indicated in the corresponding figure legends. All samples were randomly assigned to vehicle or treatment groups for the *in vitro* treatment experiments. Tumor measurements were performed blindly. The measurements of organoid shapes were analyzed blindly. For other *in vivo* and *in vitro* experiments, the researchers were not blinded while performing the experiments. No data were excluded from this study.